Efficient Quantum Dot–Quantum Dot and Quantum Dot–Dye Energy Transfer in Biotemplated Assemblies

Marc Achermann,[†,§] Sohee Jeong,[‡,§] Laurent Balet, Gabriel A. Montano, and Jennifer A. Hollingsworth*

Chemistry Division, C-PCS, Los Alamos National Laboratory, Los Alamos, New Mexico 87545, United States. [†] Present address: Lucerne University of Applied Sciences and Arts, 6048 Horw, Switzerland. [‡]Present address: Korea Institute of Machinery and Materials, 171 Jang-dong, Yuseong-gu, Daejon, 305–343, Korea. [§]These authors contributed equally to the work.

ABSTRACT CdSe semiconductor nanocrystal quantum dots are assembled into nanowire-like arrays employing microtubule fibers as nanoscale molecular "scaffolds." Spectrally and time-resolved energy-transfer analysis is used to assess the assembly of the nanoparticles into the hybrid inorganic biomolecular structure. Specifically, we demonstrate that a comprehensive study of energy transfer between quantum dot pairs on the biotemplate and, alternatively, between quantum dots and molecular dyes embedded in the microtubule scaffold comprises a powerful spectroscopic tool for evaluating the assembly process. In addition to revealing the extent to which assembly has occurred, the approach allows determination of particle-to-particle (and particle-to-dye) distances within the biomediated array. Significantly, the characterization is realized *in situ*, without need for further sample workup or risk of disturbing the solution-phase constructs. Furthermore, we find that the assemblies prepared in this way exhibit efficient quantum dot–quantum dot and quantum dot–dye energy transfer that affords faster energy-transfer rates compared to densely packed quantum dot arrays on planar substrates and to small-molecule-mediated quantum dot–dye couples, respectively.

KEYWORDS: nanocrystal quantum dots · Förster resonance energy transfer · microtubule · biotemplated assembly

The ability to construct ordered two- and three-dimensional structures on the nanometer scale is essential for the development of next-generation optical, electronic, and magnetic materials and devices. The limitations of top-down approaches in providing routes to nanoscale assembly have provided impetus for investigations of new bottom-up approaches.[1] Frequently, these latter approaches are inspired by biology and loosely based on the fundamental biological paradigm of bottom-up `self-assembly' or on specific biological structural motifs.[2] Alternatively, the approach involves direct assembly of nanomaterials using biomolecules as directing agents or as "bio-templates." A wide array of biological molecules including DNA,[3–5] viral capsids,[6] bacteriophage,[7,8] heat shock proteins,[9] and microtubules[10–12] have been used as directing agents or as templates to form two- and three-dimensionally ordered nanostructured arrays.

In this work, we study the nature and extent of association of semiconductor nanocrystals assembled using microtubule (MT) fibers as nanoscale scaffolds. Most significantly, we characterize the assembly by observing optical signatures of the assembly process induced by Förster-type energy transfer (ET) between nanocrystal quantum dots (NQDs) and between NQDs and dye molecules. Furthermore, we establish that the power of this spectroscopic technique—spectrally and time-resolved ET—to reveal the relative positions of nanoscale objects is not diminished in the biomolecular-based system. In contrast, imaging techniques, such as transmission electron microscopy (TEM) and especially high-resolution TEM, are difficult to apply to biological systems due to the high-organic content without "sterilizing" the sample by, for example, chemical or cryo-fixing, and infiltrating with a resin. Here, we show that ET methods allow *in situ* analysis in biologically relevant buffered aqueous solutions of assembly processes as well as nano-object positioning. In this way, we further validate the utility of biomolecular templates for bottom-up nanomaterials assembly and provide a novel tool based on optical spectroscopy for evaluating and ultimately utilizing the achieved assemblies.

Specifically, ET provides a mechanism for electronic "communication" between donor–acceptor (D–A) pairs by way of incoherent long-range interactions. In contrast to coherent coupling mechanisms (*e.g.*, electron tunneling) that require strong D–A interactions and a high degree of structural order, ET is far more distance and "defect" tolerant, making it an ideal candidate for exploring or exploiting interactions and assembly in biological systems. ET is characterized by an

***Address correspondence to jenn@lanl.gov.**

Received for review September 10, 2010 and accepted January 12, 2011.

Published online February 11, 2011
10.1021/nn102365v

energy-transfer rate that is dependent upon the D−A dipole coupling, which is a function of the D−A spectral overlap and has an R^{-6} near-field dependence on the D−A separation R.[13] It has been reported in a variety of NQD systems, from disordered solids[14−16] to solid-state assembled bilayers.[17,18] In each of these cases, smaller (higher energy) NQDs in the excited-state transfer their excitation energy to nearby larger (lower energy) NQDs in the ground state. Additionally, ET between NQDs and organic dye molecules has been reported.[18−20] For this work, we utilize each of these classes of "NQD ET" to investigate NQD assembly by solution-phase microtubule scaffolds. We demonstrate that ET is a versatile tool for characterizing biotemplated assemblies and that ET can be uniquely efficient in such systems.

RESULTS AND DISCUSSION

Assembly of NQDs on MTs using (Strept)avidin−Biotin Interactions. Two strategies were used to assemble MT-templated NQD structures. First, avidin-conjugated CdSe/ZnS NQDs were assembled on biotin-decorated MT scaffolds (prepared from 50% biotin-modified tubulins) by way of strong avidin−biotin interactions. Particles were successfully assembled on the MT; however, avidin-conjugated NQDs showed signs of severe, undesirable NQD−NQD aggregation that was evident in fluorescence microscopy imaging (Figure S2, Supporting Information). Avidin is highly positively charged at physiological pHs (p*I* = 10.0); therefore, nonspecific interactions with the negatively charged NQDs are expected.[21] Thus, the covalent-attachment procedure, which entailed incubation of avidin with the NQDs (see Supporting Information), likely produced not only covalently attached products but also nonspecifically bound products. The latter could involve clusters of multiple NQDs coupled electrostatically through avidin bridges that themselves could be either covalently or electrostatically bound to any given NQD. Such electrostatically mediated binding of positively charged proteins on negatively charged CdSe/ZnS NQDs has been reported previously.[22,23]

For more controlled assembly, we turned to streptavidin-conjugated NQDs (Qdot 525-ITK, Qdot Corp., CA), as streptavidin is near neutral at physiological pH.[21] Moreover, the streptavidin lacks a glycoprotein, which serves to also substantially reduce hydrophobic nonspecific interactions.[21] Therefore, we anticipated more uniform assemblies on the MT scaffolds. Indeed, as shown in Figure 1, the commercial streptavidin-conjugated NQDs assembled well on both biotinylated (50% biotinylated tubulins + 50% unlabeled tubulin) and dye-decorated MTs (25% biotinylated tubulins + 75% tetramethylrhodamine isothiocyanate (TRITC)-labeled tubulin). Significantly, a control prepared from nonbiotinylated MTs showed no templated assemblies (Figure 1d). Note: Use of greater than 50% biotinylated tubulins for the formation of MTs resulted in extensive aggregation of the MTs upon NQD assembly. The streptavidins on the NQDs possess more than one biotin-binding site, facilitating NQD-mediated MT−MT binding at such higher biotin loadings.

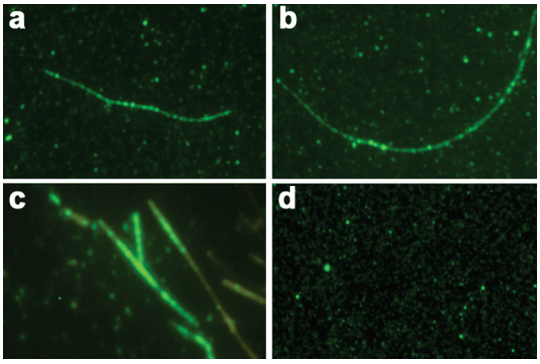

Figure 1. Optical microscope images of streptavidin-functionalized NQDs assembled onto biotinylated MT scaffolds. (a and b) 50% biotinylated MTs. (c) The 25% biotinylated and 75% TRITC-associated MTs: emission from both NQDs (green) and dye (orange) is evident. (d) Control sample: NQDs in the presence of nonbiotinylated MTs.

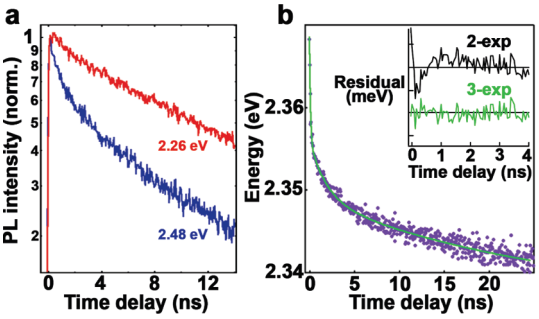

Figure 2. (a) Spectrally and time-resolved PL. Higher energy NQDs (2.48 eV PL) show faster PL decay (blue trace) compared to lower energy NQDs (2.26 eV PL; red trace), indicating energy outflow from the higher energy population to the lower energy population. (b) Dynamic red shift of the NQD average energy plotted as a function of time delay. Inset compares a triexponential fit with a double-exponential fit and reveals improved fit for the former.

NQD−NQD and NQD−Dye Energy Transfer on MT Scaffolds: Probing Assemblies at the Nanoscale. Due to the shortcomings of electron-microscopy measurement techniques (discussed above) and the resolution limits of readily available optical imaging techniques (>500 nm), NQD-MT assemblies were studied by way of spectrally and time-resolved ET measurements. Here, ET rates were extracted from analysis of exciton emission lifetimes. Specifically, faster PL decay relative to a noninteracting species indicates energy outflow (donor species), while slower PL dynamics indicate energy inflow (acceptor species). Figure 2 shows spectrally and time-resolved PL data for a quasi-size monodisperse NQD sample assembled onto MTs *via* a streptavidin−biotin linkage, where the MTs are 50% biotinylated. Within the inhomogeneously broadened PL spectrum, accelerated PL decay for smaller, higher energy NQDs (2.48 eV)

indicates that energy is being transferred out of these NQDs to the larger, lower energy NQDs (2.26 eV) in the ensemble, which show diminished PL decay indicative of energy inflow (Figure 2a). Furthermore, as shown previously,[16,17] the ET dynamics within an ensemble of quasi-monodisperse NQDs can be extracted from the dynamic redshift of the NQD average emission energy:

$$\langle E(t)\rangle = \frac{\int_0^\infty \hbar\omega \cdot I(\omega, t)\mathrm{d}\omega}{\int_0^\infty I(\omega, t)\mathrm{d}\omega} \quad (1)$$

where $I(\omega,t)$ is the PL intensity at time delay t and photon energy $\hbar\omega$. We show the energy dynamics for the MT-bound NQDs in Figure 2b. We find that the dynamics cannot be described by a single ET time but rather has a multiexponential behavior, indicating several transfer times and hence D−A distances. Comparing a double- with a triexponential fit over 40 ns reveals that only the triexponential fit accounts well for the ET dynamics over the entire time range and, in particular, within the first 2 ns (Figure 2b inset). The triexponential fit yields three well distinguishable components of similar amplitude corresponding to distinct ET times, τ_{ET}: 0.13, 2, and 20 ns with a sample-to-sample variation of ±30%. Each rate is associated with a D−A distance, r, according to the relationship:

$$r = R_0\left(\frac{\tau_{ET}}{\tau_D}\right)^{1/6} \quad (2)$$

where τ_D is the radiative lifetime (20 ns for CdSe NQDs) and R_0 = 12.7 nm is the Förster radius that has been calculated considering the refractive index of water.[24] Based on an observed 30% sample-to-sample variability in ET times and the 1/6 power dependence of r on the ET time, we calculate a 5% error for D−A distances. Therefore, the experimentally determined distances and their errors are: 5.5 ± 0.3, 8.7 ± 0.4, and 12.7 ± 0.6 nm. In considering other potential sources of error, such as those associated with the ET parameters, orientation factor and refractive index (see Supporting Information), we assume that the errors associated with these variables affect the D−A distance to a lesser extent than our 5% error derived from sample variability.

The extracted distance values compare well to distances that are predicted based on knowledge of the dimensions of the NQD and streptavidin components, *i.e.*, 5.8, 9.3, and 12.8 nm, respectively. The latter is based on an approximate NQD radius of 2.9 nm (NQD core radius of ~1.5 nm, as determined using the known correlation of the position of the NQD 1S absorption peak with NQD size, plus a ZnS shell of 0.4 nm and a polymer layer of ~1 nm, where the polymer layer thickness was determined from an analysis of literature TEM images of polymer-coated, close-packed nanoparticles)[25] and, therefore, an NQD−NQD center-to-center distance of 5.8 nm in the absence of streptavidin molecules. The streptavidin tetramer adds an additional 3−4 nm (see Supporting Information), which is doubled in the case of two intervening streptavidin molecules. It should be noted that even without the addition of MTs, a small dynamic redshift of the NQD emission is observed; however, this energy shift is substantially less pronounced than the one just described. We attribute it to ET within a small fraction of the streptavidin-conjugated NQDs that has agglomerated as a result of nonspecific binding.

Significantly, we also attempted to fit the ET dynamics with a stretched exponential function, which is often used to describe a complex system for which one expects a continuous distribution of relaxation times.[24] The stretched exponential fit described the data with χ^2 values comparable to the triexponential fit; however, we cannot justify the use of this fitting method only by the goodness of fit. Rather, given the dense NQD packing (confirmed with atomic force microscopy (AFM); Figure S3, Supporting Information), the finite size dispersion of the NQD sample (±8% obtained for a PL full-width at half-maximum (fwhm) of 30 nm centered at 527 nm), and the well-defined spacing provided by streptavidin, we do not expect a continuous distribution of ET times. For these reasons, we feel confident that the triexponential fit is the most physically accurate for this system.

To test this hypothesis, we further analyzed our assumptions as to the presence of well-defined geometries and specific NQD donor and acceptor energies that lead to well-defined ET rates. Specifically, we modeled the extent of the distributions of ET rates that result from distributions of donor−acceptor distances and spectral overlaps between donor and acceptor NQDs, which themselves result from the finite, but present, distribution of NQD sizes. If we assume that the spectral width of the PL emission is dominated by the NQD size distribution, as stated above, then we determine an 8% standard deviation for the NQD radius. For the distribution of donor−acceptor distances we consider that both donor and acceptor total sizes vary by 8% (although strictly speaking, the variation is only in the CdSe core) and that the streptavidin size is fixed at 3.5 nm. Given the sixth power dependence between donor−acceptor distance and ET rate, the rate distribution is 6 times larger than the distance distribution. Figure 3a shows the rate distributions considering the three mentioned geometries. Although the rate distribution for each configuration is sizable, there is no significant overlap between distributions of different configurations.

Similarly, we determined the distribution of ET rates caused by the distribution of spectral overlaps. For this calculation, we considered an inhomogeneous broadening of 143 meV (fwhm), a homogeneous broadening of 25 meV (fwhm), and a nonresonant Stokes shift of 80 meV. We find that the rate distribution due to

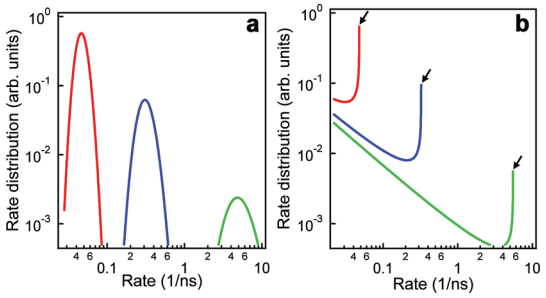

Figure 3. (a) ET rate distributions caused by variations in the donor−acceptor separation. (b) ET rate distributions caused by variations in the spectral overlap between donor emission and acceptor absorption energies. In both (a) and (b) we considered equally weighted contributions from three donor−acceptor geometries with nominal separations of 5.8 (green traces), 9.3 (blue traces), and 12.8 (red traces) nm. In (b), peak rates of the three configurations are indicated by arrows.

spectral overlap variations for a fixed geometry peaks at a rate that corresponds to perfect overlap between donor emission and acceptor absorption spectra (Figure 3b). Unfavorable spectral overlap is the cause for the tail at very small ET rates that can lead to slow components in the ET dynamics. However, if we assume that the different donor−acceptor configurations as introduced above are possible, the ET dynamic is dominated by the peak rates of the three configurations, since the probability of the peak rate corresponding to a configuration with a larger D−A separation is always higher than the probability of the same rate associated with smaller D−A separations (as evident in Figure 3b).

The described method of using observations of ET between NQDs to monitor their assembly on a MT backbone works well if a dense coverage of NQDs on the MTs can be achieved or is desirable. For the opposite case, where the NQD coverage is low, the average distance between NQDs is increased, and ET is suppressed, rendering this approach ineffective for assessing MT-mediated NQD assembly. For this situation, we suggest an alternative method that relies on ET between NQDs and dye molecules that are bound to the tubulin proteins. Here, we used TRITC dye as our ET acceptor, as this molecule has an absorption spectrum that overlaps well with the emission spectrum of the streptavidin-NQDs. The excellent spectral overlap affords efficient NQD-to-dye ET when the NQD and dye are sufficiently close, enabling use of NQD-TRITC ET as an indicator of NQD binding to the MT scaffold. Again, we use spectrally and time-resolved PL measurements to reveal the ET dynamics. In Figure 4a we show the NQD PL dynamics obtained from NQD/TRITC-MT assemblies after subtracting the PL contribution from any unbound NQDs. This PL decay is compared to reference NQDs in the absence of the dye ET acceptors and is found to be significantly faster. As inter-NQD ET does not occur at the low concentrations used here, we conclude that the additional decay channel is caused by NQD-TRITC ET. This conclusion is also supported by measurements of the acceptor PL dynamics. In our experiment, the TRITC dye molecules can produce PL either because of ET from excited NQDs or by direct laser excitation (the dye absorption at the laser excitation wavelength of 402 nm is small but finite). In Figure 4b, we compare the PL decay of solely dyes with the PL dynamics measured from dyes in the assemblies (after subtracting the PL contribution from dyes that are directly excited by the laser pulse). The dye PL dynamics in the NQD/TRITC-MT assemblies show a delayed rise that is complementary to the decay dynamics of the NQD donors and, therefore, can be explained by energy inflow from the NQDs, supporting the assertion of NQD-TRITC ET.

For a quantitative analysis of the ET process, we further analyze the NQD donor dynamics. Specifically, ET adds an additional decay channel to the donor PL decay that can be written as

$$PL_D(t) = PL_D^0(t) \sum_k a_k e^{-t/\tau_k} \quad (3)$$

where PL_D^0 is the donor PL dynamics in the absence of ET and τ_k is the ET time of a fraction a_k of NQDs that has a specific distance r_k to the dye acceptor molecules. [Comment: the equation is independent of the donor PL dynamics, *i.e.*, it holds equally well for both high- and low-quantum yield NQDs, where the latter is characterized by NQD subensembles that decay either radiatively or nonradiatively with different decay rates and, therefore, exhibit multiexponential dynamics.] Hence, in Figure 4c, we plot $PL_D(t)/PL_D^0(t)$ *versus* the time delay and show directly the time-resolved NQD-TRITC ET dynamics. We can clearly discriminate two distinct ET dynamics, a fast and a slow one with time constants of 90 ps and 8 ns, respectively, that we determine from a double exponential fit. The existence of two dynamics indicates that two D−A geometries have to be considered. Then, using the equation for energy dynamics (eq 2) and a NQD-TRITC dye Förster radius, R_0, of 6.6 nm (for its calculation, see ref 24), we determine the D−A distances to be 2.7 and 5.7 nm. From Figure 4c, we are also able to extract the fraction of NQDs that are bound to the MT backbone as well as the relative numbers of NQDs that are positioned closely to TRITC dyes (*i.e.*, 2.7 nm and faster ET) or farther away (*i.e.*, 5.7 nm and relatively slower ET). Specifically, we find that ~two-thirds of the NQDs are bound to the MTs, leaving ~one-third of the NQDs unbound (constant PL ratio at long time delays in Figure 4c). Of the bound NQDs, we observe that the vast majority sits closely to TRITC molecules (~90%), while a minority (~10%) resides at the longer separation distance (as obtained from the relative amplitudes of the two exponential functions that were fit to the PL ratio in Figure 4c). The shorter distance corresponds to

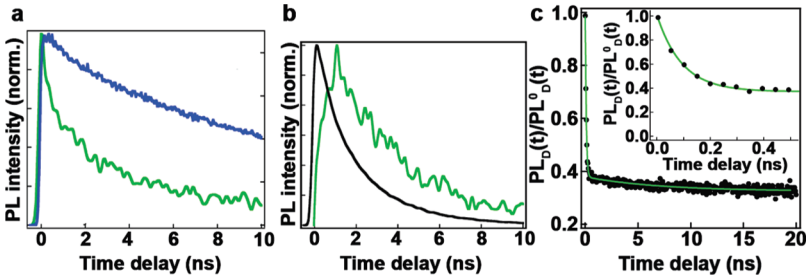

Figure 4. (a) NQD emission dynamics at 530 nm in the absence (blue trace) and presence (green trace) of TRITC dye molecules. Comparison of the measurements shows that NQD emission is quenched in the presence of TRITC-labeled biotinylated MTs. (b) Dye emission at 640 nm directly excited (black trace) and indirectly excited by way of ET from NQDs (green trace). The delayed rise in the green trace indicates ET from NQD donors. (c) Ratio of donor PL dynamics in the presence and absence of ET. Inset enlarges data points within the first 0.5 ns after excitation. The green solid line indicates the double exponential fit.

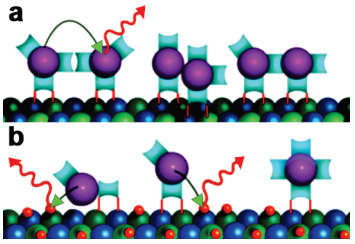

Figure 5. Schematic illustration of (a) NQD−NQD and (b) NQD−dye spatial relationships resulting in observed ET dynamics. NQDs are depicted by purple spheres, streptavidin by blue hourglass shapes, and dye molecules by red spheres. The blue and green spheres represent the MT backbone.

NQDs bound directly to the MT scaffold with the streptavidin linker off to the side (*i.e.*, approximately the radius of the NQD including its inorganic and organic shells), while the longer distance corresponds roughly to this distance plus a separation distance of one intervening streptavidin (see below).

Distances Obtained from ET Measurements Provide Insight into Nanoscale Structures of the NQD Assemblies. The three D−A distances extracted from NQD−NQD ET measurements (5.5, 8.7, and 12.7 nm) suggest specific spatial arrangements for the streptavidin-conjugated NQDs on biotinylated MT backbones. The longest distance, 12.6 nm, corresponds well to ET between two NQDs that are separated by two streptavidins (~12.8 nm), where the NQD radii contribute ~5.5 nm combined and each streptavidin contributes ~3.5 nm. Note: Here we are assuming streptavidins approach the NQD and each other by way of their shortest dimension, the ~3.5 nm "waist" of an hourglass molecular shape (Figures 5a and S4, Supporting Information).[26] The middle ET distance, 8.7 nm, corresponds well to ET between two NQDs that are separated by one streptavidin (~9.3 nm), again positioned such that the NQD fits into the "waist" of the streptavidin molecule. Alternatively, the longest observed ET distance (12.6 nm) could be accounted for by a single streptavidin that is positioned such that its longest axis provides the NQD−NQD separation (5.8 nm),[26] though this scenario yields a somewhat shorter distance (only ~11.3 nm: 5.5 nm from two NQD radii plus 5.8 nm from one streptavidin along its long axis) than is observed by our ET measurements. Thus, while it remains unclear the exact structure and orientation of the NQD-bound streptavidins, it is apparent that the ET-derived distances are reflective of likely streptavidin-mediated separations (*i.e.*, considering both the shortest and longest dimensions of the protein). Lastly, with more confidence, we assert that the shortest observed ET distance (5.8 nm) results from the scenario whereby no streptavidins are positioned between the NQD pairs (Figure 5a). Importantly, with the exception of the scenario for which two streptavidins intervene between NQD pairs, each of the scenarios implies that streptavidin coverage of the NQD surfaces is incomplete. Only for the case of incomplete coverage could NQDs approach each other directly or with one streptavidin intervening.

The extraction of multiple D−A distances from the NQD−dye ET measurements (2.7 and 5.7 nm) also implies variations due to apparently incomplete streptavidin coverage. Specifically, the longer distance corresponds to a separation distance of one intervening streptavidin, with the approach by way of the streptavidin's narrow "waist". The fast component, accounting for the majority of the ET that is taking place, corresponds best to NQD−dye ET that is not hindered by any intervening streptavidin spacer. This observation indicates that most of the NQDs are bound directly to the MT scaffold with any streptavidin linkers off to the side (Figure 5b, left). Significantly, compared to previously reported attempts to assemble NQD−dye ET-active solution-phase ensembles using a protein intermediate, the ET observed here is fast. We obtain an ET rate of 90 ps for the "majority" fast component, compared to literature values of 1−4 ns.[18,19] We suggest that our faster ET is a direct result of using the solution-phase scaffold to facilitate assembly. In our case, the protein "intermediate" or linker can situate off to the side, facilitated by incomplete surface coverage of the NQD by the protein, allowing almost direct contact between the D−A NQD-dye pair.

In each of these cases (NQD−NQD and NQD−dye ET analyses), we postulated the different geometries

(NQD−NQD and NQD−dye distances) based on the different observed ET dynamics without considering the possibility of multiple acceptors. It is known that the ET efficiency improves as a function of the number of acceptors.[17−19] Thus, if in our case multiple acceptors were present for a particular donor, then our determinations of different donor−acceptor distances based on differences in ET dynamics would be complicated by this additional influence on ET rates. Indeed, it was previously shown that in an ideal hexagonal array, as is formed by a perfectly close-packed Langmuir−Blodgett monolayer of like-sized NQDs, there exist 3 "shells" of acceptor NQDs surrounding a donor NQD, where shells 1−3 comprise 6, 12, and 18 possible acceptor NQDs, respectively.[17] However, for MT-mediated assembly, we do not anticipate a perfectly formed close-packed monolayer but, rather, only a densely packed irregular one. Thus, the longer range ordering is absent, and the multiple "shells" are replaced by one "shell" comprising NQDs that have different separations to a center donor NQD, the different distances that we observe. In this scenario, it is possible that for one donor NQD, there are ∼two NQDs in the exact same configuration, but it is unlikely that both such NQDs would be good acceptor NQDs, *i.e.*, provide the necessary spectral overlap of donor emission with acceptor absorption, given the tight size (and, therefore, energy) distribution of the sample.

In the case of NQD−dye ET, the dye molecules are sufficiently separated (4 nm along the length of the MT and 6 nm along the circumference), such that ET occurs predominantly from an NQD to the closest dye molecule, assuming that there is only one dye (or fewer) per tubulin unit. This assumption is accurate given that there are 1−2 dyes per tubulin (information provided by Cytoskeleton, Inc.), and we are using only 50% dye-labeled tubulin for the MT polymerization procedure (see Methods), providing a dye/tubulin ratio of 0.5−1.0. Lastly, in neither case are our ET measurements complicated by the presence of nonspecific NQD aggregation. We used AFM to confirm that the NQDs assembled onto the MTs as densely packed monolayers without hint of agglomeration or significant gap formation (Figure S3, Supporting Information). Furthermore, as described above, streptavidin-conjugated NQDs were shown by analysis of spectrally and time-resolved ET dynamics to be mostly stable against solution-phase self-aggregation.

In conclusion, we have shown that spectrally and time-resolved ET analysis is a useful spectroscopic tool for assessing the biomediated assembly of optically active nanoparticles *in situ* and that the assemblies afford efficient NQD−NQD and NQD−dye ET. Hybrid inorganic biological systems, such as the NQD-MT assemblies studied here, are of fundamental interest due to their potential for combining the distinct properties of dissimilar systems into a single construct toward realization of novel, coupled properties. For example, in NQD-MT assemblies, NQD emission properties are combined with the MT structural templating property, where assembly can be either static or dynamic[27] or in further combination with biological "motors" (*e.g.*, kinesin motor proteins), afford directed transport of nanoparticle cargo.[28−30] These interesting systems often pose challenges to more traditional characterization approaches, including solution-phase techniques that cannot accurately assess structurally and size-complex systems (*e.g.*, dynamic light scattering) and solid-state techniques that currently require removal of constructs from the relevant solution environment (*e.g.*, TEM). In contrast, advanced ET analyses are able to unequivocally demonstrate the existence of NQD assembly as well as provide a semiquantitative understanding of the extent of the assembly (bound *vs* unbound) and the nature of the nanoscale structure (NQD−NQD and NQD−dye distances). Lastly, the biomolecular template (MT) was shown to be an effective platform for coupling NQD−NQD and NQD−dye D−A pairs. The MT scaffold provided more efficient (faster) NQD−NQD ET compared to that observed for a similarly sized and monodisperse NQD sample that was prepared instead by dropcasting onto a flat glass substrate.[16] Similarly, NQD−dye ET was considerably faster compared to that afforded by protein linkers (90 ps compared to 1−4 ns), where the imperfect streptavidin coating likely permitted essentially direct contact between the NQD and an accepting dye molecule without compromising the required streptavidin−biotin coupling.

METHODS

Tubulin, biotinylated tubulin, and TRITC-labeled tubulin proteins were purchased from Cytoskeleton, Inc., Denver, CO, as the lyophilized form (>99% pure). In both cases, biotinylated tubulin and TRITC-labeled tubulin, labeling was achieved through covalently binding to random surface lysines at a one-to-one stoichiometry with the tubulin subunits.[31] All tubulins were stored at −70 °C in 4 μL aliquots after suspension in MT polymerization buffer (BRB80-P, 5 mg/mL; see below). Taxol (paclitexel; 2 mM in dimethylsulfoxide) and guanosine 5′-triphosphate (GTP) (100 mM) solutions were also purchased from Cytoskeleton, Inc., Denver, CO, and diluted as necessary. All buffers were made in the lab according to the following procedures.

BRB80 was prepared from 80 mM piperazine-*N*,*N*′-bis[2-ethanesulfonic acid] sodium salt (PIPES), 1 mM ethylene glycol-bis(b-amino-ethyl ether) *N*,*N*,*N*,*N*′-tetraacetic acid (EGTA), and 1 mM $MgCl_2$ and then adjusted to pH 6.9. BRB80-P (polymerization buffer) was prepared from BRB80, 1 mM GTP, and 10% glycerol. BRB80-T (taxol buffer) was prepared form BRB80 to which 1% (by volume) 2 mM taxol had been added.

Streptavidin-conjugated quantum dots (Qdot 525-ITK, 530 nm emission) were purchased from Quantum Dot Corp., Hayward, CA, stored without dilution, and used without further purification. All other chemicals were purchased from Aldrich.

Avidin-conjugated, polymer-encapsulated CdSe−ZnS core−shell NQDs were prepared in-house (see Supporting Information for experimental details) and compared to the streptavidin-conjugated NQD system in terms of their ability to form "high-quality" biotemplated assemblies (see Results and Discussion). CdSe−ZnS core−shell NQDs were synthesized using established colloidal synthetic techniques.[32,33] The NQDs were then rendered water-soluble by encapsulation in an amphiphilic polymer shell terminated with negatively charged carboxyl groups following modified literature procedures.[34,35] The polymer-coated NQDs were subsequently cross-linked using a lysine cross-linking procedure to improve the stability of the coating. Avidin was then conjugated to the cross-linked NQDs.

MTs were formed by polymerizing tubulin. Different ratios of unlabeled and labeled tubulin were used depending upon the experiment. Aliquots (of "tubes") of tubulin were thawed by placing in room-temperature water for 30 s. The tubulin was then placed on ice. For experiments involving NQD−NQD and NQD-Au NP assemblies, each tube would contain 50% unlabeled tubulin and 50% biotinylated tubulin. For NQD−dye experiments, tubes containing 75% TRITC-labeled tubulin and 25% biotinylated tubulin were prepared. In all cases, the total protein used for polymerization was 20 μg. Total volume of the polymerization reaction was adjusted to 4−20 μL with BRB80-P, and additional glycerol was added when the protein concentration was low (10% of the total volume was used for 5 mg/mL solutions and increased up to 20% for 1 mg/mL reactions to ensure efficient polymerization). Polymerization was effected by incubating the tubes at 37 °C for 20 min. While the tubulin was polymerizing, BRB80-T was warmed to 37 °C, and 250 μL was then added to the MT solution to stabilize the polymerized MTs with respect to dynamic instability.[29] Stable for only 2−3 h, the tubes were quickly removed from the water bath and used immediately for nanoparticle assembly. NQDs were assembled onto biotinylated MTs by adding 2 mL of streptavidin-conjugated NQDs (2 mM) to the buffered MT solutions and incubating for 15 min with gentle shaking at room temperature. Removal of free dyes from the purchased TRITC-labeled tubulin was conducted using a Micro Bio-Spin column (Bio-Gel P 30, Bio-Rad, CA) after equilibration of the gel matrix with BRB80-T. The concentration of tubulins (and therefore biotin) was approximately 3 μM, and the streptavidin (or avidin) concentration provided by addition of the NQDs (see below) was also approximately 3 μM (assuming 5 streptavidins/avidins per NQD).

In some cases, higher MT stabilities were desired. Additional stabilization was provided by cross-linking the formed MTs using gluteraldehyde.[36] MTs were polymerized from tubulin and stabilized with BRB80-T, as described in the previous section. Gluteraldehyde was then added to a final concentration of 10 mM and incubated at room temperature with shaking for 2 h. To remove unreacted gluteraldehyde, the product was run through a spin column (Bio-Gel P-30), which was pre-equilibrated with BRB80-T.

NQDs were assembled onto the MTs as follows. After polymerization of 20 μg tubulin, 2 μg of MT product was removed and diluted with 10 μL of BRB80-T. The biotinylated MTs were mixed with 2 μL streptavidin-NQDs (Qdot 525-ITK, 2 μM) or with 2 μL avidin-NQDs (CdSe/ZnS-avidin NQDs synthesized in-house, 2 μM) and incubated for 30 min with gentle shaking at room temperature.

Success of the biotemplated NQD-assembly process was initially confirmed using optical microscopy. MT-NQD solutions were diluted with BRB80-T and placed on a poly-(L)-lysine-coated glass slide. Coverslips were placed on top of the solution, and fluorescence images were viewed after 5 min with an Olympus IX71 inverted microscope and a Nikon PlanFluor 100x oil emersion objective (N.A. = 1.30). Images were collected with a CCD camera (Q-Fire, Olympus America Inc., Melville, NY). For detecting TRITC-labeled MTs, antifade solution was added to the sample to reduce photobleaching.

Using spectrally and time-resolved PL spectroscopy, dynamical studies of ET were undertaken to assess the assembly of NQDs on the MT scaffolds. Samples were prepared in PEG-coated cuvettes (to prevent adhesion to the cuvette walls) at 5 μM concentrations (tubulin dimer: 110 kDa). The samples were excited at 402 nm (3.1 eV) with 50 ps pulses from a pulsed diode laser (Picoquant LDH-P-C-400). The PL was spectrally dispersed in a monochromator (Acton Research SpectraPro 300i with a 600 grooves/mm grating) with a spectral resolution of 1.25 nm and detected with a cooled multichannel plate photomultiplier tube (Hamamatsu R3809U-51). The detection system was coupled to a time-correlated single photon counting system (Becker-Hickl SPC-630). The laser and detection systems provided a 70 ps time resolution in time-resolved PL measurements.

Acknowledgment. We thank G. Bachand, Sandia National Laboratories, for helpful discussions pertaining to MT assembly and maintaining MT stability. The work was supported by Los Alamos National Laboratory Directed Research and Development Funds, especially those dedicated to start-up activities of the Center for Integrated Nanotechnologies, a U.S. Department of Energy, Office of Basic Energy Sciences user facility. J.H. acknowledges partial support through NIH-NIGMS grant 1R01GM084702-01. S.J acknowledges partial support from the Nano R&D program, grant 2009-0083219.

Supporting Information Available: FTIR spectra, fluorescence microscope images, atomic force microscope (AFM) images, additional ET data, and expanded discussions of ET-associated errors. This material is available free of charge *via* the Internet at http://pubs.acs.org.

REFERENCES AND NOTES

1. Lu, W.; Lieber, C. M. Nanoelectronics from the Bottom Up. *Nat. Mater.* **2007,** *6*, 841–850.
2. Shimizu, T.; Masuda, M.; Minamikawa, H. Supramolecular Nanotube Architectures Based on Amphiphilic Molecules. *Chem. Rev.* **2005,** *105*, 1401–1443.
3. Mitchell, G. P.; Mirkin, C. A.; Letsinger, R. L. Programmed Assembly of DNA Functionalized Quantum Dots. *J. Am. Chem. Soc.* **1999,** *121*, 8122–8123.
4. Mirkin, C. A.; Letsinger, R. L.; Storhoff, J. J. A DNA-based Method for Rationally Assembling Nanoparticles into Macroscopic Materials. *Nature* **1996,** *382*, 607–609.
5. Warner, M. G.; Hutchison, J. E. Linear Assemblies of Nanoparticles Electrostatically Organized on DNA Scaffolds. *Nat. Mater.* **2003,** *2*, 272–277.
6. Fowler, C. E.; Shenton, W.; Stubbs, G.; Mann, S. Tobacco Mosaic Virus Liquid Crystals as Templates for the Interior Design of Silica Mesophases and Nanoparticles. *Adv. Mater.* **2001,** *16*, 1266–1269.
7. Lee, S.-W.; Mao, C.; Flynn, C. E.; Belcher, A. M. Ordering of Quantum Dots Using Genetically Engineered Viruses. *Science* **2002,** *596*, 892–895.
8. Mao, C.; Flynn, C. E.; Hayhurst, A.; Sweeney, R.; Qi, J.; Georgiou, G.; Iverson, B.; Belcher, A. M. Viral Assembly of Oriented Quantum Dot Nanowires. *Proc. Natl. Acad. Sci. U. S.A.* **2003,** *100*, 6946–6951.
9. McMillan, R. A.; Paavola, C. D.; Howard, J.; Chan, S. L.; Zaluzec, N. J.; Trent, J. D. Ordered Nanoparticle Arrays Formed on Engineered Chaperonin Protein Templates. *Nat. Mater.* **2002,** *1*, 247–252.
10. Behrens, S.; Wu, J.; Habicht, W.; Unger, E. Silver Nanoparticle and Nanowire Formation by Microtubule Templates. *Chem. Mater.* **2004,** *16*, 3085–3090.
11. Bachand, G. D.; Rivera, S. B.; Boal, A. K.; Gaudioso, J.; Liu, J.; Bunker, B. C. Assembly and Transport of Nanocrystal CdSe Quantum Dot Nanocomposites Using Microtubules and Kinesin Motor Proteins. *Nano Lett.* **2004,** *4*, 817–821.
12. Jeong, S.; Hollingsworth, J. A. Polymerization of Nanocrystal Quantum Dot-Tubulin Bioconjugates. *IEEE Trans. Nanobioscience* **2006,** *5*, 239–245.
13. Förster, T. Energiewanderung und Fluoreszenz. *Naturwissenschaften* **1946,** *33*, 166–175.

14. Kagan, C. R.; Murray, C. B.; Nirmal, M.; Bawendi, M. G. Electronic Energy Transfer in CdSe Quantum Dot Solids. *Phys. Rev. Lett.* **1996,** *76*, 1517–1520.
15. Micic, O. I.; Jones, K. M.; Cahill, A.; Nozik, A. J. Optical, Electronic, and Structural Properties of Uncoupled and Close-Packed Arrays of InP Quantum Dots. *J. Phys. Chem. B* **1998,** *102*, 9791–9796.
16. Crooker, S. A.; Hollingsworth, J. A.; Tretiak, S.; Klimov, V. I. Spectrally Resolved Dynamics of Energy Transfer in Quantum-Dot Assemblies: Towards Engineered Energy Flows in Artificial Materials. *Phys. Rev. Lett.* **2002,** *89*, 186802–186804.
17. Achermann, M.; Petruska, M. A.; Crooker, S. A.; Klimov, V. I. Picosecond Energy Transfer in Quantum Dot Langmuir-Blodgett Nanoassemblies. *J. Phys. Chem. B* **2003,** *107*, 13782–13787.
18. Clapp, A. R.; Medintz, I. L.; Mauro, J. M.; Fisher, B. R.; Bawendi, M. G.; Mattoussi, H. Fluorescence Resonance Energy Transfer between Quantum Dot Donors and Dye-Labeled Protein Acceptors. *J. Am. Chem. Soc.* **2004,** *126*, 301–310.
19. Medintz, I. L.; Clapp, A. R.; Mattoussi, H.; Goldman, E. R.; Fisher, B.; Mauro, J. M. Self-Assembled Nanoscale Biosensors Based on Quantum Dot FRET Donors. *Nat. Mater.* **2003,** *2*, 630–638.
20. Zhou, D.; Piper, J. D.; Abell, C.; Klenerman, D.; Kang, D.-J.; Ying, L. Fluorescence Resonance Energy Transfer between a Quantum Dot Donor and a Dye Acceptor Attached to DNA. *Chem. Commun.* **2005,** 4807–4809.
21. Green, M. N. Avidin and Streptavidin. *Methods Enzymol.* **1990,** *184*, 51–67.
22. Mattoussi, H.; Mauro, J. M.; Goldman, E. R.; Anderson, G. P.; Sundar, V. C.; Mikulec, F. V.; Bawendi, M. G. Self-assembly of CdSe-ZnS Quantum Dot Bioconjugates Using an Engineered Recombinant Protein. *J. Am. Chem. Soc.* **2000,** *122*, 12142–12150.
23. Pinaud, F.; King, D.; Moore, H.; Weiss, S. Bioactivation and Cell Targeting of Semiconductor CdSe/ZnS Nanocrystals with Phytochelatin-Related Peptides. *J. Am. Chem. Soc.* **2004,** *126*, 6115–6123.
24. Lakowicz, J. R. *Principles of Fluorescence Spectroscopy*, 2nd ed.; Kluwer Academic: New York, 1999.
25. Pellegrino, T.; Manna, L.; Kudera, S.; Liedl, T.; Koktysh, D.; Rogach, A. L.; Keller, S.; Rädler, J.; Natile, G.; Parak, W. J. Hydrophobic Nanocrystals Coated with an Amphiphilic Polymer Shell: A General Route to Water Soluble Nanocrystals. *Nano Lett.* **2004,** *4*, 703–707.
26. Hendrickson, W. A.; Pahler, A.; Phizackerley, R. P. Crystal-Structure of Core Streptavidin Determined from Multiwavelength Anomalous Diffraction of Synchrotron Radiation. *Proc. Natl. Acad. Sci. U.S.A.* **1989,** *86*, 2190–2194.
27. Liu, H.; Spoerke, E. D.; Bachand, M.; Koch, S. J.; Bunker, B. C.; Bachand, G. D. Biomolecular Motor-Powered Self-Assembly of Dissipative Nanocomposite Rings. *Adv. Mater.* **2008,** *20*, 4476–4481.
28. Hancock, W. O. Intracellular Transport: Kinesins Working Together. *Curr. Biol.* **2008,** *18*, R715–R717.
29. Hess, H.; Clemmens, J.; Qin, D.; Howard, J.; Vogel, V. Light-Controlled Molecular Shuttles Made from Motor Proteins Carrying Cargo on Engineered Surfaces. *Nano Lett.* **2001,** *1*, 235–239.
30. Hiyama, S.; Gojo, R.; Shima, T.; Takeuchi, S.; Sutoh, K. Biomolecular-Motor-Based Nano- or Microscale Particle Translocations on DNA Microarrays. *Nano Lett.* **2009,** *9*, 2407–2413.
31. Hyman, A. A.; Drexel, D.; Kellog, D.; Mitchison, T. J. Preparation of Modified Tubulins. *Methods Enzymol.* **1991,** *196*, 478–485.
32. Murray, C. B.; Norris, D.; Bawendi, M. G. Synthesis and Characterization of Nearly Monodisperse CdE (E = S, Se, Te) Semiconductor Nanocrystallites. *J. Am. Chem. Soc.* **1993,** *115*, 8706–8715.
33. Hines, M. A.; Guyot-Sionnest, P. Synthesis and Characterization of Strongly Luminescing ZnS-Capped CdSe Nanocrystals. *J. Phys. Chem. B* **1996,** *100*, 468–471.
34. Wu, X.; Liu, J.; Liu, K. N.; Haley, J. A.; Bruchez, M. P. Immunofluorescent Labeling of Cancer Marker Her2 and Other Cellular Targets with Semiconductor Quantum Dots. *Nat. Biotechnol.* **2003,** *21*, 41–46.
35. Jeong, S.; Achermann, M.; Nanda, J.; Ivanov, S.; Klimov, V. I.; Hollingsworth, J. A. Effect of the Thiol−Thiolate Equilibrium on the Photophysical Properties of Aqueous CdSe/ZnS Nanocrystal Quantum Dots. *J. Am. Chem. Soc.* **2005,** *127*, 10126–10127.
36. Gaskin, F. Techniques for the Study of Microtubule Assembly Invitro. *Methods Enzymol.* **1982,** *85*, 433–439.